LA-UR- 99-788

Approved for public release; distribution is unlimited.

Title: METEOROLOGICAL SIMULATIONS OF OZONE EPISODE CASE DAYS DURING THE 1996 PASO DEL NORTE OZONE STUDY

Author(s): M. J. Brown, K.Costigan, C. Muller, Ge Wang

Submitted to: Air & Waste Management Assoc, St. Louis, MO, 6/20-24/99

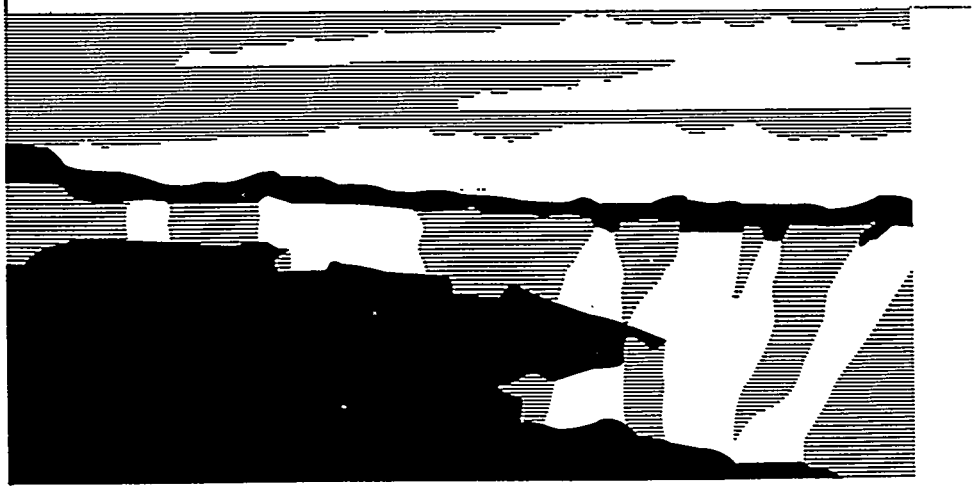

Los Alamos
NATIONAL LABORATORY

DISCLAIMER

Portions of this document may be illegible in electronic image products. Images are produced from the best available original document.

Meteorological Simulations of Ozone Episode Case Days During the 1996 Paso del Norte Ozone Study

99-189

Michael J. Brown

Energy & Environmental Analysis, Los Alamos National Laboratory, Los Alamos, NM 87545

Keeley Costigan

Atmospheric & Climate Sciences, Los Alamos National Laboratory, Los Alamos, NM 87545

Cathrin Muller

Nuclear System Design & Analysis, Los Alamos National Laboratory, Los Alamos, NM 87545

Ge Wang

Mechanical and Aerospace Engineering, Arizona State University, Tempe, AZ 85287

ABSTRACT

Meteorological simulations centered around the border cities of El Paso and Ciudad Juarez have been performed during an ozone episode that occurred on Aug. 13, 1996 during the 1996 Paso del Norte Ozone Study field campaign. Simulations were performed using the HOTMAC mesoscale meteorological model using a 1, 2, 4, and 8 km horizontal grid size nested mesh system. Investigation of the vertical structure and evolution of the atmospheric boundary layer for the Aug. 11-13 time period is emphasized in this paper. Comparison of model-produced wind speed profiles to rawinsonde and radar profiler measurements shows reasonable agreement. A persistent upper-level jet was captured in the model simulations through data assimilation. In the evening hours, the model was not able to produce the strong wind direction shear seen in the radar wind profiles. Based on virtual potential temperature profile comparisons, the model appears to correctly simulate the daytime growth of the convective mixed layer. However, the model underestimates the cooling of the surface layer at night. We found that the upper-level jet significantly impacted the turbulence structure of the boundary layer, leading to relatively high turbulent kinetic energy (tke) values aloft at night. The model indicates that these high tke values aloft enhance the mid-morning growth of the boundary layer. No upper-level turbulence measurements were available to verify this finding, however. Radar profiler-derived mixing heights do indicate relatively rapid morning growth of the mixed layer.

INTRODUCTION

Sharing the same airshed, the U.S. and Mexican cities of El Paso and Ciudad Juarez violate their respective national ambient air quality standards for ozone. As part of the La Paz Agreement Annex 5, the U.S. and Mexico have consented to monitor and study the air basin, and determine air quality reduction strategies for these border cities. In order to quantify the air quality and

meteorological parameters during ozone episodes, a major field study was performed in the El Paso/Ciudad Juarez airshed during the summer of 1996. During the field study, the one hour ozone standard was exceeded on Aug. 13 and a near violation occurred on Sept. 4. As part of the Paso del Norte Study, we are simulating the meteorology of the days surrounding these two events with the HOTMAC and RAMS mesoscale meteorological codes using a system of nested grid meshes. Our goal is to utilize both the field measurements and model simulation results to better understand the circulation patterns in the El Paso/Ciudad Juarez region. In addition, the model-produced meteorological fields will be used to drive photochemical air chemistry models. In this paper, we concentrate our efforts on HOTMAC model simulations of the Aug. 11-13 time period. We begin with short descriptions of the El Paso/Ciudad Juarez modeling domain, the prevailing weather patterns, and the Paso del Norte field experiment. In the next section, we briefly describe the HOTMAC meteorological code and modeling parameters. We then provide a summary of the mesoscale meteorological flow fields and the boundary-layer evolution produced by the model for this time period. Initial comparisons between model results and data are shown and interesting phenomenon and model-data differences are highlighted.

BACKGROUND

The Paso del Norte Region

Ciudad Juarez and El Paso are located in close proximity to where the borders of Texas, New Mexico and Mexico meet (fig. 1). The meteorological modeling domain for this project covers southeastern New Mexico, northwestern Texas, and northern Chihuahua. As shown in the outermost modeling grid of the HOTMAC domain (fig. 2), the Sacramento Mountains and the Black Range bound the northern-half of the domain to the east and west, respectively, while the foothills of the Sierra Madre demarcate the southwestern edge of the domain. The Tularosa Basin is defined by the Sacramento Mountains to the east and the San Andres Mountains to the west. The Rio Grande River flows primarily from north to south in the Jornada del Muerte between the San Andres and the Black Range, and then south of Ciudad Juarez the river flows southeast. The land cover in this region is dominated by desert scrubland, except for the forest-covered Sacramento and Black Range mountains (see landuse map for the outermost HOTMAC grid, fig. 3a).

The Rio Grande separates El Paso to the north from Ciudad Juarez to the south. El Paso wraps around the southern tip of the Franklin Mountains, while Ciudad Juarez extends westward onto the foothills of the Sierra Juarez and spreads south-southeast following the Rio Grande. The urban areas are surrounded by desert scrubland, except for irrigated regions along the Rio Grande (see landuse map for the innermost HOTMAC grid, fig. 3b). The topography used for these simulations was obtained from the USGS 3-second U.S. and 30-second global DEM datasets. Landuse for the U.S. side of the border was derived from the USGS LULC dataset, while landuse on the Mexican side of the border was obtained from a combination of 1:100,000 and 1:50,000 scale topographical maps. The landuse data is known to have been last updated with 1970's aerial photographs, so that we expect our estimated urban coverage to be underestimated.

The 1996 Paso del Norte Ozone Study Field Campaign

The Paso del Norte Ozone Study field campaign was conducted from July to September during the summer of 1996. It was a multi-agency effort led by the USEPA Region VI and the Texas Natural Resource Conservation Commission and coordinated by Sonoma Technologies Inc. A wide variety of surface and upper-level air quality measurements were taken and are described elsewhere in this session.[1] Routine daily meteorological measurements were collected from twice daily NWS balloon soundings at Santa Teresa International Airport (about 20 km west of El Paso) and at twenty surface meteorological stations in El Paso, Ciudad Juarez, and in surrounding communities. Three radar wind profilers with radio acoustic sounding systems (RASS) provided hourly-averaged vertical profiles of wind speed, wind direction, and virtual temperature and were located at positions running north to south adjacent to the Rio Grande (see fig. 4, the terrain map of the HOTMAC innermost grid). Vertical profiles of wind speed and direction are available from one sodar located near the southern edge of El Paso. In addition, measurements from an instrumented aircraft and hot air balloon were collected during the intensive operating periods when ozone episodes were forecasted. A thorough description of the field experiment dataset can be found in the 1996 Paso del Norte Ozone Study Final Report.[2]

Weather Patterns During the August Episode

The dominant weather feature in the region at the time of the August 13th ozone episode in El Paso/Juarez was the upper-level high pressure ridge. Several days earlier, on August 8th, a broad area of relatively large geopotential heights covered most of the southern two-thirds of the United States at the 500 mb pressure level. Along the northern tier of states, height contours were zonal. Over the next several days the 500 mb pattern changed, with a ridge remaining over the western U. S. and a relative trough developing over the eastern U. S. By the morning of August 12th, the greatest heights on the 500 mb surface were centered over central Utah. This high slowly expanded and moved to the south and east and was centered over the four corners area on August 13th. El Paso and Juarez were in the southeastern portion of this high and were under the influence of northeasterly winds at 500 mb. Beginning on the 14th, the ridge slowly weakened. These conditions are historically related to ozone producing episodes.[3]

At the surface, high pressure and relatively weak surface winds dominated the large-scale conditions in the southwestern U. S. Most disturbances remained far to the north and traveled along the Canadian border. During this time period, the highest surface pressures in El Paso were recorded on the 13th. Interestingly, the rawinsonde profiles from the Santa Teresa International Airport show significant high speed winds aloft. The jet reaches a maximum wind speed of nearly 22 m/s at 3000 m above ground level (agl) at 6 a.m. on Aug. 12 and then over the next several days ascends in height and reduces strength slightly. As will be shown later, the upper-level jet may play a significant role in daytime boundary-layer development.

MODEL DESCRIPTION

HOTMAC Model

HOTMAC (Higher-Order Turbulence Model for Atmospheric Circulation) is a three-dimensional

time-dependent mesoscale meteorological model.[4] Using the hydrostatic approximation, a gradient-diffusion closure scheme for the horizontal turbulence components, and a terrain-following coordinate system, the governing conservation equations for mass, momentum, heat, and moisture are solved numerically using the alternating direction implicit (ADI) finite difference scheme. The last two terms in the horizontal momentum equations (1) and (2) are forest/urban canopy drag and nudging terms, respectively. The forest and urban canopy drag terms account for the sub-grid momentum sink resulting from flow around trees and buildings.[5,6] The nudging term allows the model to run in a quasi-diagnostic mode when the nudge coefficient G is large or it allows the model to account for boundary conditions when G is small. In our simulations G is set to 0.0004, sufficiently small to make the nudging term one of the weaker forcing terms in the momentum equations.[4] The radius-of-influence term f(x,y,z) has a Gaussian distribution with maximum value one at the observation location (x_0,y_0) and a horizontal standard deviation that is a function of height z. This allows one to have nudging near the surface influence only a very small area where observed winds are most likely representative of a smaller area and at upper-levels influence a larger area where observed winds are likely representative of a larger area.

Equation 1. Prognostic momentum equation for east-west component of wind velocity.

$$\frac{\partial \overline{U}}{\partial t}+\overline{U}\frac{\partial \overline{U}}{\partial x}+\overline{V}\frac{\partial \overline{U}}{\partial y}+\overline{W}\frac{\partial \overline{U}}{\partial z}=f\left(\overline{V}-\overline{V}_g\right)+g\frac{\overline{H}-z^*}{\overline{H}}\left[1-\frac{\left\langle\overline{\Theta}_v\right\rangle}{\overline{\Theta}_v}\right]\frac{\partial z_g}{\partial x}+\frac{\partial}{\partial x}\left[K_{xx}\frac{\partial \overline{U}}{\partial x}\right]+\frac{\partial}{\partial y}\left[K_{xy}\frac{\partial \overline{U}}{\partial y}\right]$$
$$+\frac{\overline{H}}{H-z_g}\frac{\partial}{\partial z^*}\left(-\overline{uw}\right)-\eta C_d a\left(z^*\right)\overline{U}\left|\overline{U}\right|+G_u\cdot f(x,y,z)\cdot\left(U_{obs}-\overline{U}\right)$$

Equation 2. Prognostic momentum equation for north-south component of wind velocity.

$$\frac{\partial \overline{V}}{\partial t}+\overline{U}\frac{\partial \overline{V}}{\partial x}+\overline{V}\frac{\partial \overline{V}}{\partial y}+\overline{W}\frac{\partial \overline{V}}{\partial z}=-f\left(\overline{U}-\overline{U}_g\right)+g\frac{\overline{H}-z^*}{\overline{H}}\left[1-\frac{\left\langle\overline{\Theta}_v\right\rangle}{\overline{\Theta}_v}\right]\frac{\partial z_g}{\partial y}+\frac{\partial}{\partial x}\left[K_{xy}\frac{\partial \overline{V}}{\partial x}\right]+\frac{\partial}{\partial y}\left[K_{yy}\frac{\partial \overline{V}}{\partial y}\right]$$
$$+\frac{\overline{H}}{H-z_g}\frac{\partial}{\partial z^*}\left(-\overline{vw}\right)-\eta C_d a\left(z^*\right)\overline{V}\left|\overline{V}\right|+G_v\cdot f(x,y,z)\cdot\left(V_{obs}-\overline{V}\right)$$

The vertical momentum, heat, and moisture fluxes are approximated using a one-equation 1.5 order turbulence closure scheme, where the turbulent length scale (l_m) is determined from an algebraic equation and the turbulent kinetic energy (tke) is solved numerically by an approximated prognostic differential equation.[4] Equation (3) shows the relationship for the Reynolds shear stresses. It is important to note that the turbulent length scale l_m is modified by a term S_m which is a function of stability (Richardson number). However, the length scale used in the dissipation term in the tke prognostic equation is not stability corrected. This latter point will be of importance in the Results & Discussion section below.

Equation 3. The turbulence closure relationship for the Reynolds shear stress terms.

$$\left[\overline{uw},\overline{vw}\right]=-l_m\cdot\tilde{S}_M\cdot\sqrt{2\cdot tke}\cdot\left[\frac{\partial \overline{U}}{\partial z},\frac{\partial \overline{V}}{\partial z}\right]$$

The lower boundary conditions are defined by similarity theory and a surface energy balance between short- and longwave energy and sensible, latent, and soil heat fluxes. The two-stream delta-eddington method is used to solve for the incoming shortwave energy flux,[7] while a prescribed surface albedo determines the outgoing shortwave flux. The upward and downward longwave radiation fluxes are determined using the Stefan-Boltzmann relation and the method of Sasamori, respectively.[8] The sensible heat flux is obtained from similarity theory, while the latent heat flux is computed from a daytime-prescribed and nighttime-computed Bowen ratio. The soil heat flux is obtained by solving a 5-level heat conduction equation in the soil which ignores lateral heat transfer.

Problem Setup

The meteorological simulation was performed using a nested four grid horizontal mesh system composed of 32 x 66, 30 x 30, 40 x 40 and 40 x 50 grids of size 8, 4, 2 and 1 km's, respectively. Figures 2 and 4 depict the outermost 8 km grid mesh and the innermost 1 km grid mesh, respectively. Twenty-one vertical grid levels were used, with spacing (in terrain-following coordinates) of 5 m's for the lowest four cells and expanding to a maximum of 720 m's at the model domain top. The domain extends 6000 m's above ground level (agl) in terrain-following coordinates.

The meteorological simulations began at 6:00 pm on Aug. 11, 1996 and lasted roughly thirty-six hours. The initial conditions for the simulations were obtained from the local airport rawinsonde sounding. Horizontal homogeneity was imposed on the initial meteorological fields since we are using only one vertical profile; hence, some spin-up time is needed to allow the model to overcome the over-simplified starting conditions. In order to capture the upper-level jet and the changing synoptic conditions, a data assimilation scheme using the rawinsonde and radar wind profiler data taken at 12 and 6 hour intervals, respectively, was used to "nudge" the winds. The nudging radius-of-influence linearly increased from 1 km at the ground to 500 km at the domain top; however, nudging was turned off *below* 500 meters agl.

RESULTS AND DISCUSSION

Mesoscale Flow Features

Figure 5 shows the nighttime flow patterns near the surface on the outermost grid at 12 midnight on Aug. 13, thirty hours after the simulation start time. We see strong topographic influences, as well as the effect of large-scale synoptic forcing apparent in the generally easterly flow. Drainage off the eastern side of the Sacramento Mountains is offset by the prevailing wind. However, drainage flows off the western slopes of the Sacramentos combine with the prevailing wind to provide strong easterly flow over the Tularosa Basin. These winds converge with the weaker drainage winds off the San Andres and result in winds flowing north to south along the western edge of the basin. Likewise, drainage winds off the eastern side of the Black Range converge with the prevailing easterly winds which results in some north to south channeling along the Jornada del Muerte. A thin elongated strip of light winds blowing parallel to the Rio Grande River Valley is found south of Ciudad Juarez.

Zooming in to the innermost grid, we can see that convergence of drainage flows over the city center results in light winds there and perhaps a vortex-type recirculation (fig. 6). Although the upper-level winds are relatively strong at this time, stable stratification disconnects the low-level flow from the faster moving upper-level flow. The drainage winds off the eastern-side of the Franklin mountains converge with the Tularosa Basin winds resulting in a narrow region of northerly flow just east of the Franklins. Prior modeling efforts indicates that the location of the convergence zones changes based on the strength and direction of the upper-level prevailing winds.

At noon on Aug. 12, all the surface-level winds travel in the same direction as the prevailing upper-level winds (fig. 7). According to the model, the influence of local features (e.g., mountain upslope flow) is being overwhelmed by the large-scale forcing. Strong turbulent mixing is bringing the faster moving horizontally-homogeneous winds down to the surface. Initial analysis of surface level stations indicates more spatial variability in wind direction, but low-level radar winds indicate uniformity in the wind direction. The wind speed reduction over the city area is due to canopy drag.

Boundary-Layer Evolution

The model simulation suggests relatively strong growth of the boundary layer in the morning hours. The model-computed potential temperature profiles in fig. 8a show strong ground-level cooling at night, but an isothermal region remains aloft. During morning hours as the ground is heated, the boundary layer grows eating away at the stable layer (fig. 8b). Once reaching the isothermal layer, the convective boundary layer grows rapidly without impedance. The turbulent kinetic energy (tke) profile shows large values aloft at night (fig. 8c). Typically, the tke decreases at night due to stable stratification, but the strong wind shear associated with the upper-level jet produces mechanically-created turbulence in the model's turbulent closure scheme. This might explain the well-mixed temperature profile aloft at night and the rapid boundary-layer growth in the morning. Whether an isothermal region remains aloft at night in reality is debatable; as we show in the next section, the RASS data does not extend high enough for corroboration. Whether the large tke values found aloft at night are real cannot be verified as well. We note that tke might possibly decay at a faster rate at night if the length scale l_m found in the denominator of the tke dissipation term was scaled by stability parameter S_m as done by several authors.[9]

Model-Data Comparisons

Wind Profiles. In this section, we compare the model results to the vertical profiles of wind speed and direction measured by the rawinsonde and radar profiler. The first twelve hours of the model simulation are not used to allow for model spin-up. Figures 9a-d show comparisons at six hour intervals. The upper-level jet is well reproduced, but this is due to nudging, not model physics (we believe that the upper-level jet is synoptically produced and therefore should be a boundary condition for the smaller-scale HOTMAC model). Although the model-computed profiles follow the general trend of the measurements, it is clear that there are some major differences. For a given hour, the model wind speed profiles are nearly the same at each of the three radar sites (ELD, ELE, ELW) and the rawinsonde site, whereas the measurements generally

show small, but consistent differences at each site (e.g., figs. 9a and b). Both the model and field data show a fairly well-mixed wind speed profile typical of daytime convective boundary layers at 12 noon on Aug. 12 (fig. 9a). At 6 pm, the model does not capture the "S" shape found in the radar data; however, the rawinsonde data does not have the "S" shape either (fig. 9b). At midnight, the model simulates a nocturnal jet peaking at the 400-500 meter level, whereas the data shows it several hundred meters higher and 2-3 m/s faster (fig. 9c). At 6 am, the model produces a low-level jet with roughly the same magnitude as found in the radar measurements, but the radar data shows the jet 400-500 meters higher in elevation (fig. 9d).

The model agrees fairly well with the radar-measured wind direction profiles at 12 noon on Aug. 12 (fig. 10a). At 6 pm, the radar measurements show more wind direction shear with height than found in the model-computed profiles and the rawinsonde profile (fig. 10b). Although the model is being nudged towards the measured radar winds at site ELE, the remnants of the convective boundary layer mixing are apparently overwhelming the nudging term in the model equations. At midnight, the radar data reveals a very strong wind direction shear between 1000 and 2000 meters (fig. 10c). The model does not capture the strong shear and the winds in the lowest 1000 meters are off by nearly 30 degrees. At 6 am, the radar data again shows extremely strong wind direction shear between 1000 and 2000 meters (fig. 10d). The model-computed wind direction profile more closely resembles the rawinsonde measurements, however.

Temperature Profiles. The model temperature field has been initialized using the rawinsonde sounding taken at 18 lst on Aug. 11. Eighteen hours later at 12 noon, the model predicts slightly warmer temperatures than those measured by the RASS units (fig. 11a). It should be pointed out that, in general, the RASS temperatures appear to be 1-2 degrees cooler than those from the rawinsonde. At 6 pm, the model computed temperature profile matches the rawinsonde data well (fig. 11b). The top of the well-mixed layer is clearly visible at 3200-3400 m agl. As evidenced by the profiles at 12 midnight and 6 am, the model significantly underpredicts the cooling in the lowest one thousand meters (figs. 11c and d). It is possible that our scrubland land classification contains too much moisture which regulates cooling at night. Initial comparisons with surface temperature time series measurements tends to support this hypothesis. Note that in fig. 11d the rawinsonde profile has a very different character than the RASS data. In general, the rawinsonde and RASS temperature profiles on other mornings compared favorably and tended to look more like the RASS data seen in fig. 11d.

CONCLUSIONS

We have compared meteorological simulations computed by the HOTMAC model to data collected during the 1996 Paso del Norte Ozone Study field campaign. Model-produced wind speed profiles showed reasonable agreement with rawinsonde and radar profiler measurements, but in the evening hours, the model was not able to produce the strong wind direction shear seen in the observations. The model appears to correctly simulate the daytime growth of the convective mixed layer, but underestimates the cooling of the nighttime surface layer. We found that a persistent upper-level jet significantly impacted the turbulence structure of the boundary layer, leading to relatively high turbulent kinetic energy values aloft at night and enhancing the

mid-morning growth of the boundary layer. We will next compare model results to surface-based meteorological measurements and low-level sodar-derived wind fields. In addition, we will begin using the RAMS meteorological model which will allow us to ingest more meteorological information into the simulation and look at the effect of large-scale subsidence on the boundary-layer growth.

Acknowledgements. This work was funded by USEPA Region VI. We would like to thank Jim Yarbrough of USEPA Region VI for his support of this project; Paul Roberts and Clinton MacDonald for advice and help with the experimental datasets; Victor Valenzuela for tours of the meteorological stations in El Paso and Ciudad Juarez, and Mike Williams, Pete Breitenbach, and Dick Karp for insightful advice on meteorological conditions and modeling.

REFERENCES

1. Roberts, P., C. MacDonald, H. Main and D. Coe: *The 1996 Paso del Norte Ozone Study: An Overview of the Field Study and Data Analyses*, 92nd Annual AWMA Meeting, St. Louis, June 1999.
2. Roberts, P., D. Coe, T. Dye, S. Ray, and M. Arthur: Summary of measurements obtained during the 1996 Paso del Norte ozone study, Final Report, STI-996191-1603-FR, 1996.
3. Roberts, P., C. MacDonald, H. Main, T. Dye, D. Coe, T. Haste: Analysis of Meteorological and Air Quality Data For the 1996 Paso del Norte Ozone Study, Final Report, STI-997330-1754-FR, 1997.
4. Yamada, T. and S. Bunker: *A numerical model study of nocturnal drainage flows with strong wind and temperature gradients*, J. Appl. Meteor., 28, pp 545-554, 1989.
5. Yamada, T.: A numerical study of turbulent airflow in and above a forest canopy, J. Meteor. Soc. Japan, 60, pp 111-126, 1982.
6. Brown M. and M. Williams: *An urban canopy parameterization for mesoscale meteorological models*, AMS 2nd Urban Env. Symp., Albuquerque, NM, 1988.
7. Smith W. and C. Kao: *Numerical simulations of observed Arctic stratus clouds using a second-order turbulence closure model*, J. Appl. Meteor., 35, pp 47-59, 1996.
8. Sasamori, T.: *The radiative cooling calculation for application to general circulation experiments*, J. Appl. Meteor., 7, pp 721-729, 1968.
9. Arritt, R.: *The effect of water surface temperature on lake breezes and thermal internal boundary layers*, Bound. Layer Meteor., 40, pp 101-125, 1987.

Figure 1. Map showing location of El Paso and Ciudad Juarez.

Figure 2. Topography found in the HOTMAC outermost grid mesh (8 km resolution).

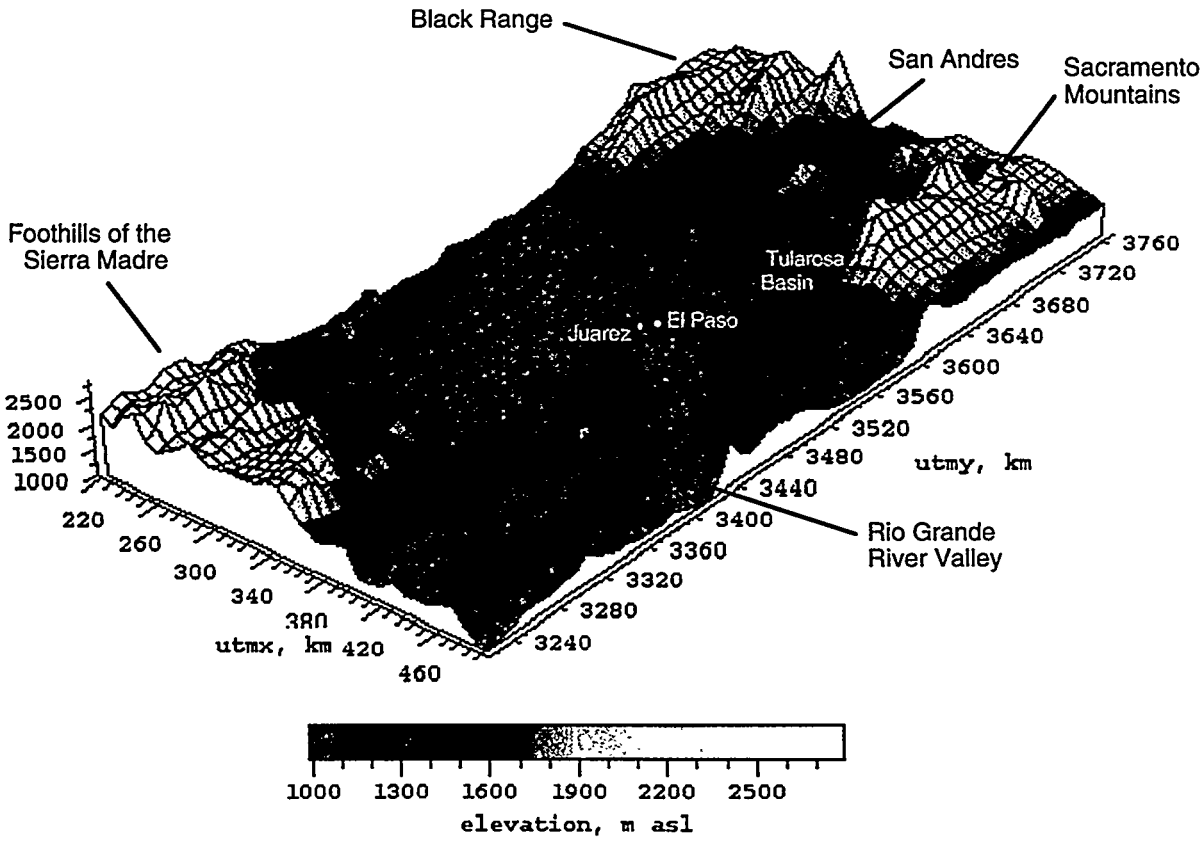

Figure 3. a) Land use map for the HOTMAC outermost grid mesh (8 km resolution) and b) the innermost grid mesh (1 km resolution).

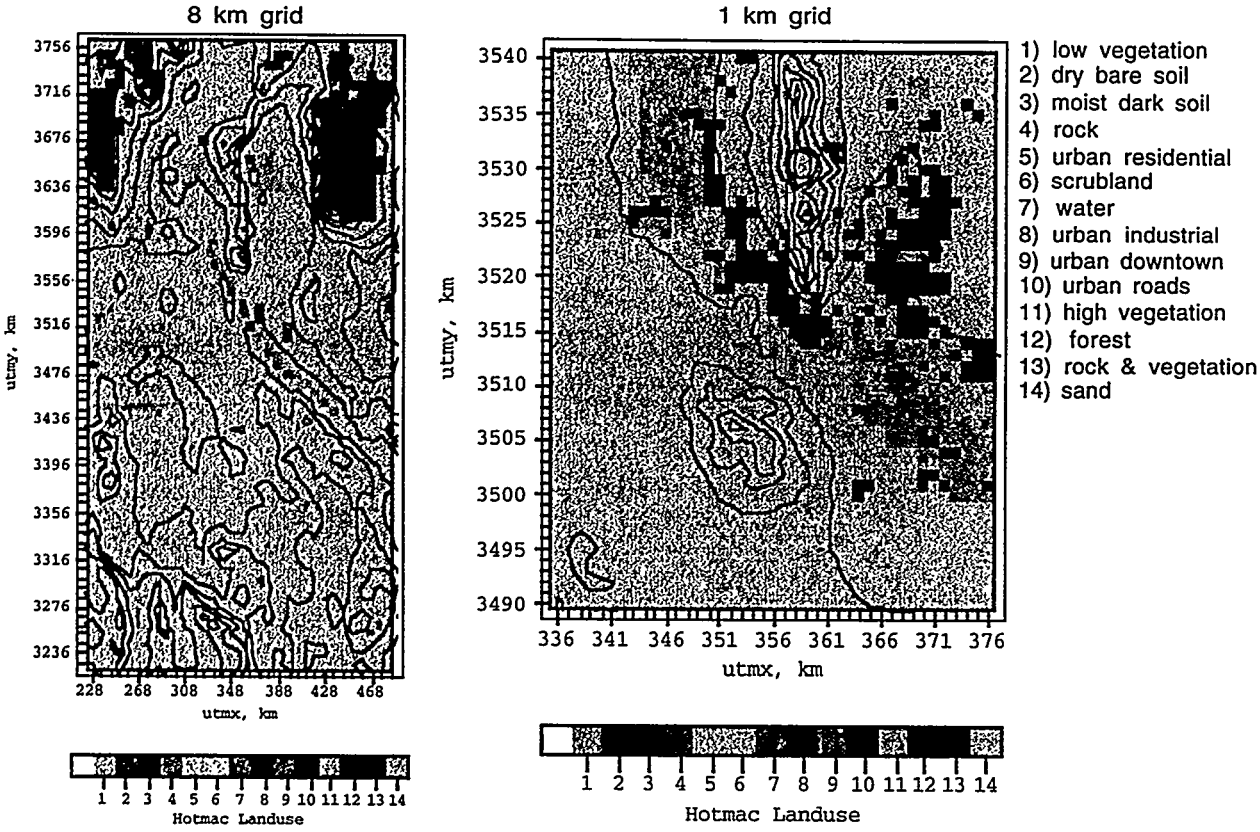

Figure 4. Topography found on the HOTMAC innermost grid mesh (1 km resolution).

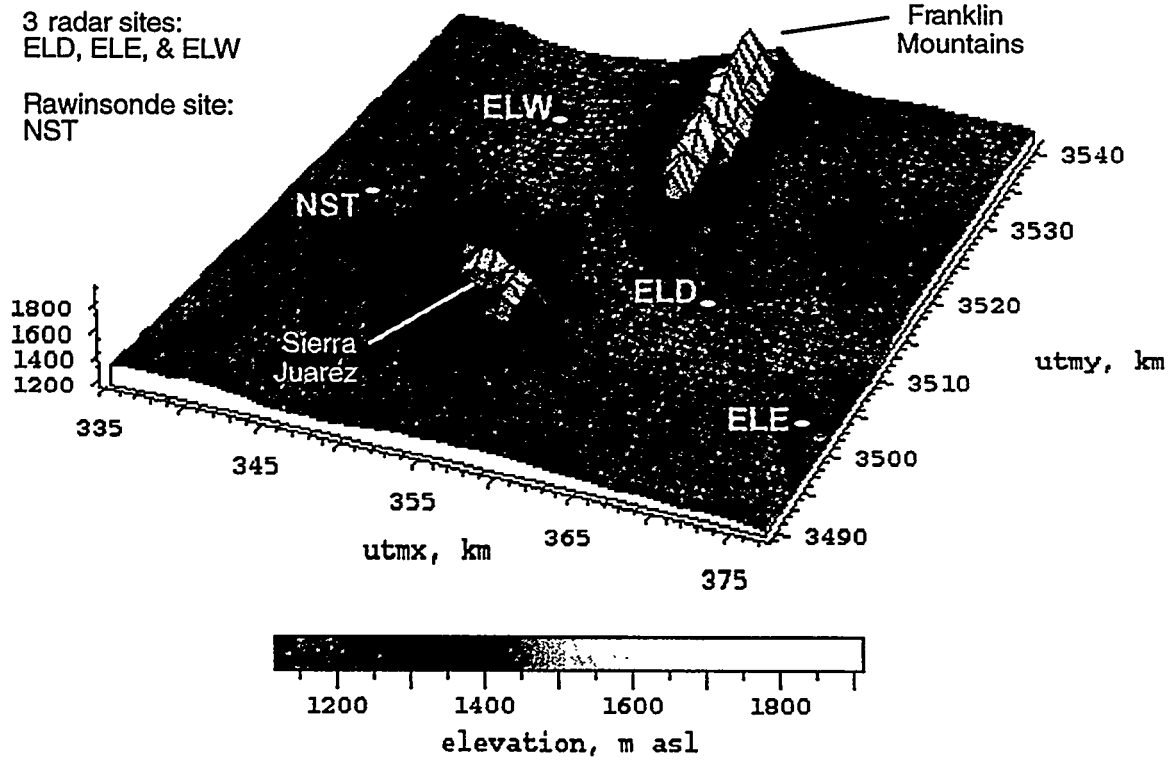

Figure 5. Surface wind field on the outermost grid mesh at 12 midnight on Aug. 13.

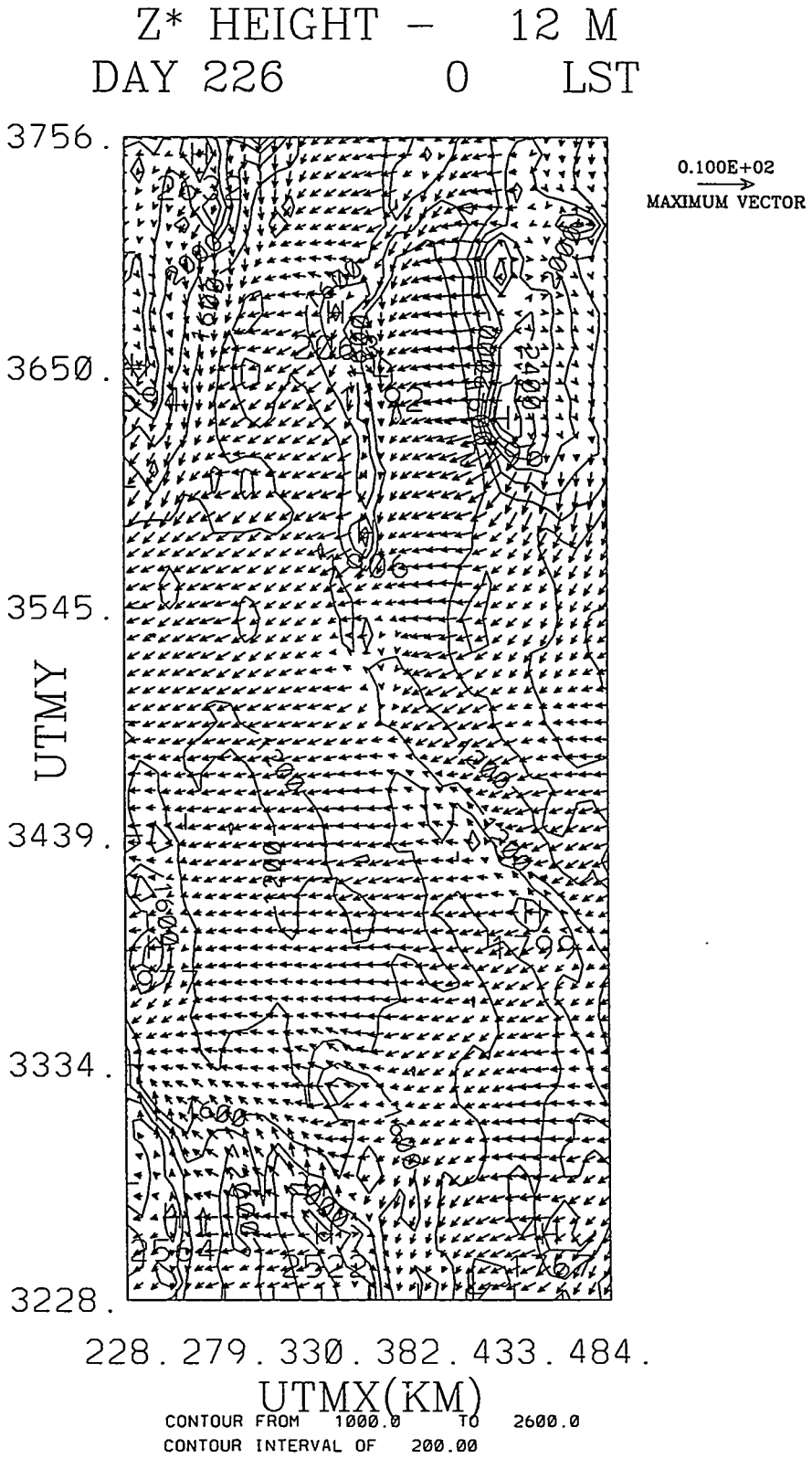

Figure 6. Surface wind field on the innermost grid mesh at 12 midnight on Aug. 13.

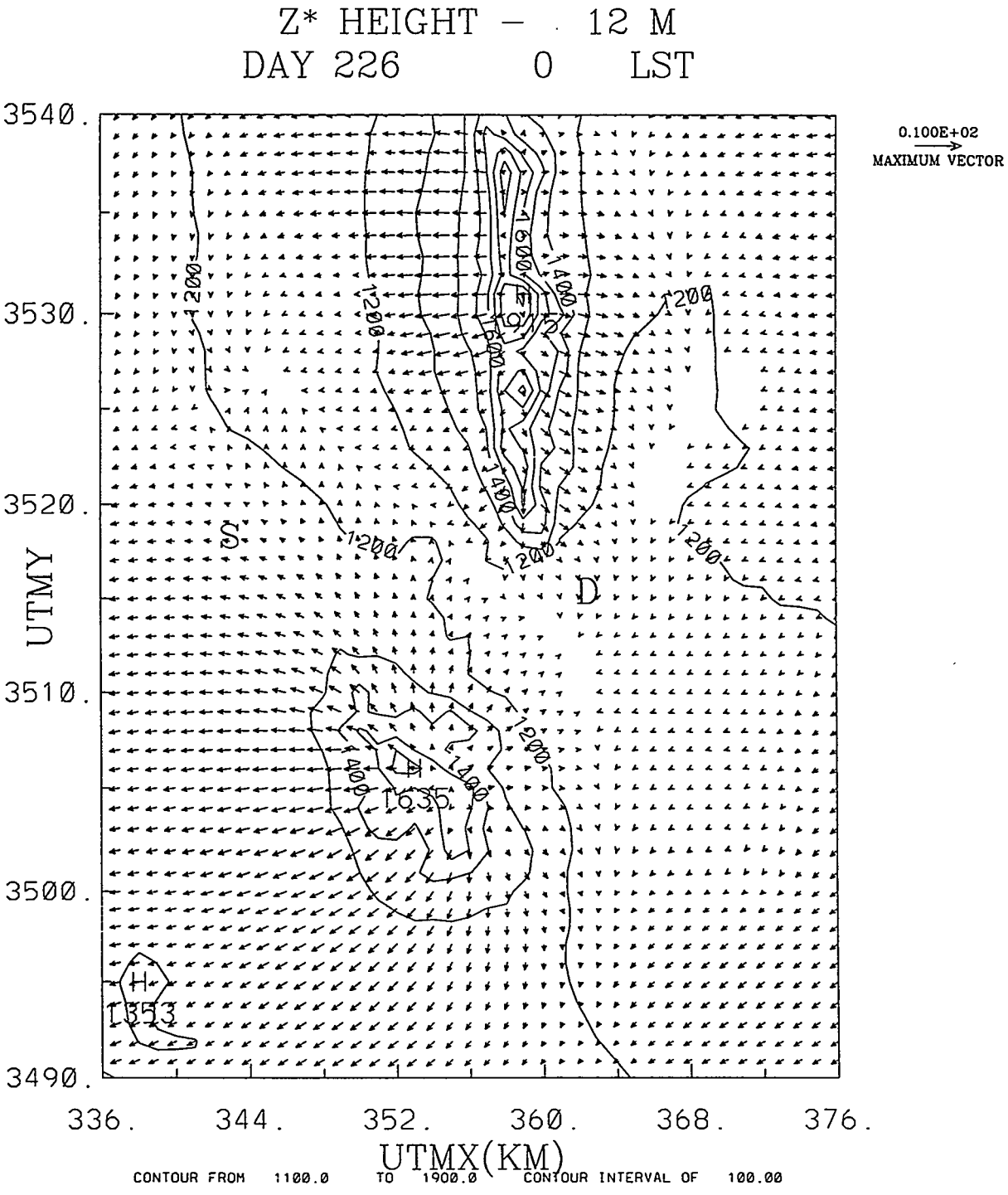

Figure 7. Surface wind field on the innermost grid mesh at 12 noon on Aug. 12.

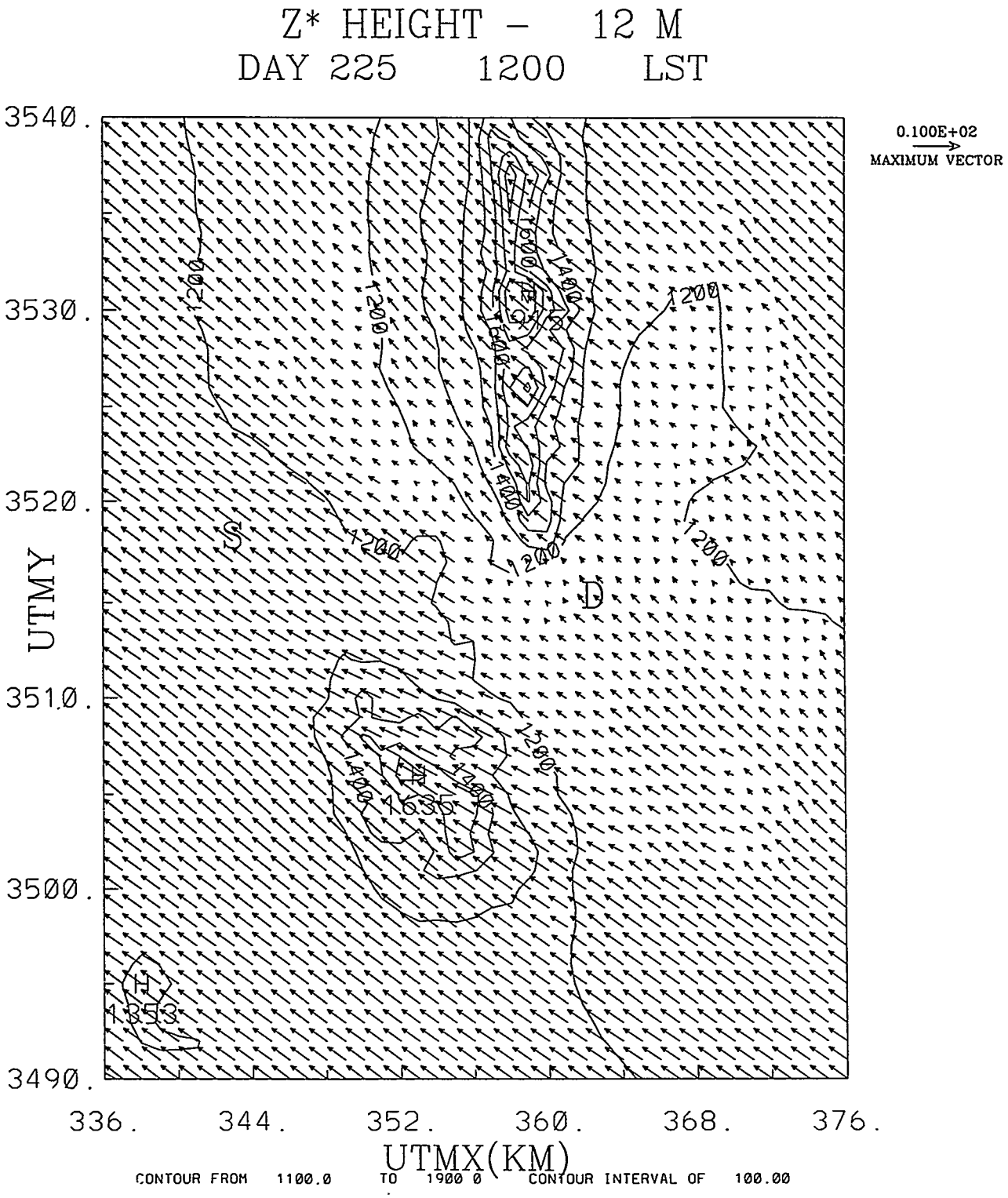

Figure 8. Boundary-layer evolution computed by the model: a) potential temperature profiles during the night and b) during the daytime; and c) turbulent kinetic energy profiles at night.

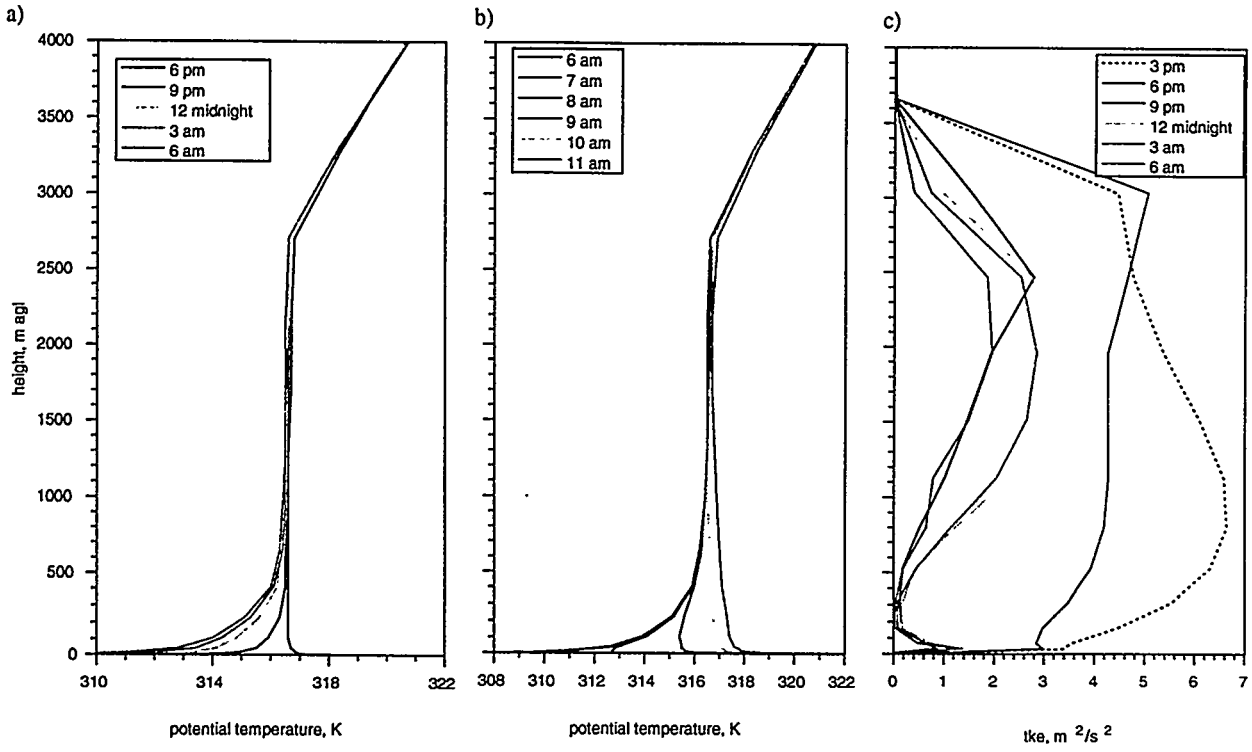

Figure 9. Comparison of model-computed wind speed profiles and field measurements for: a) 12 noon, b) 6 pm, c) 12 midnight and d) 6 am.

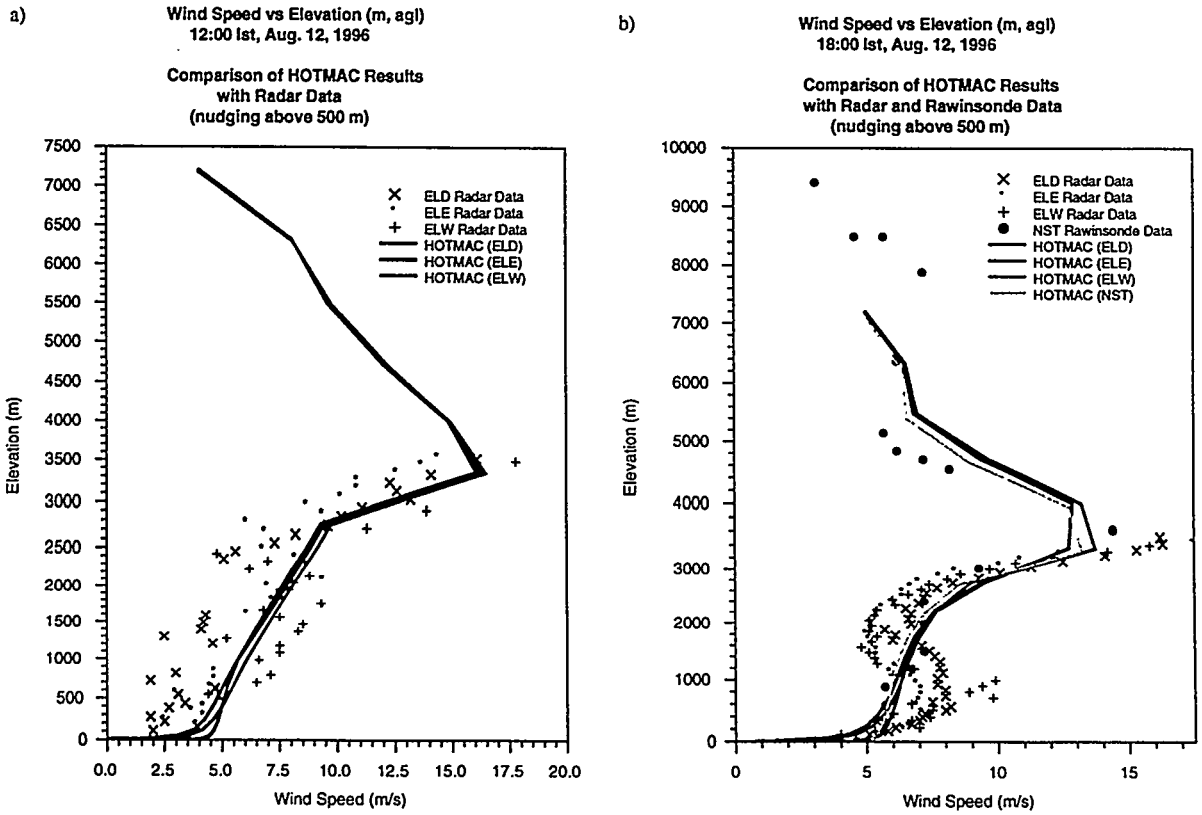

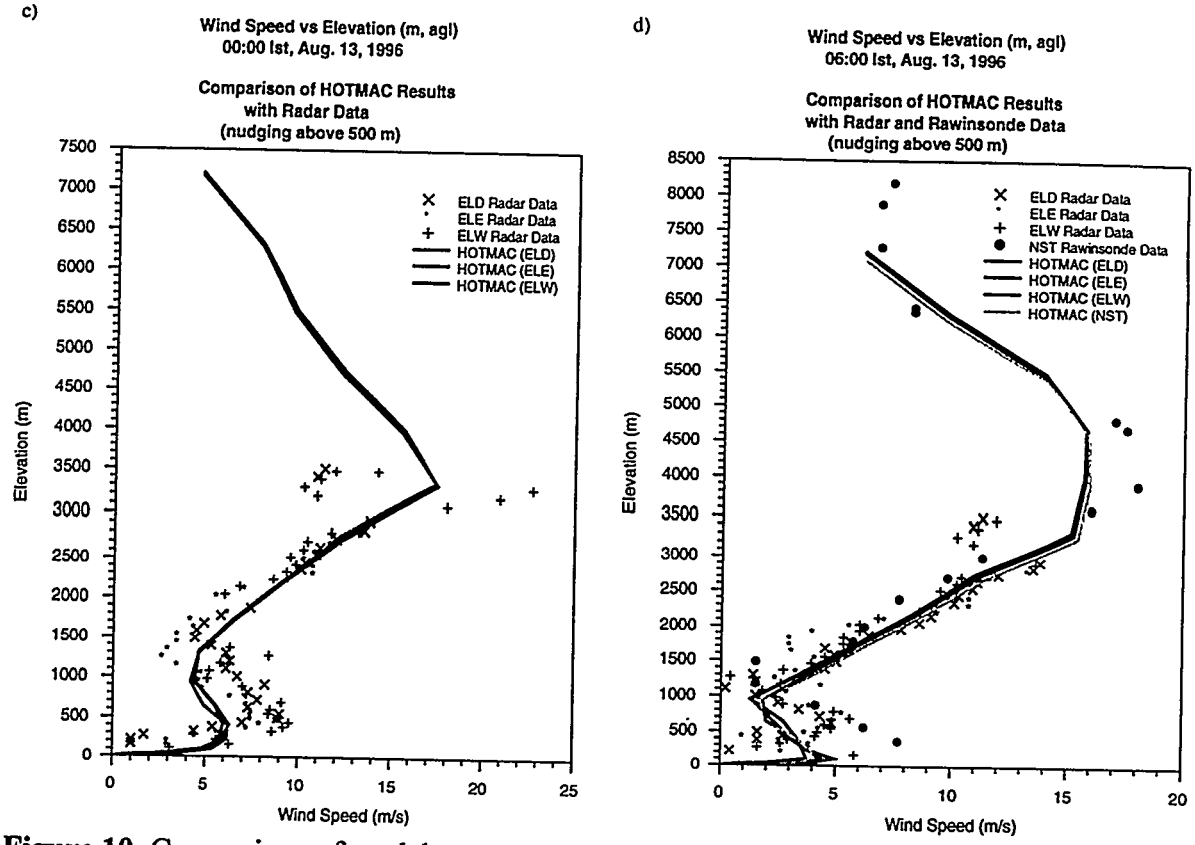

Figure 10. Comparison of model-computed wind direction profiles and field measurements for: a) 12 noon, b) 6 pm, c) 12 midnight and d) 6 am.

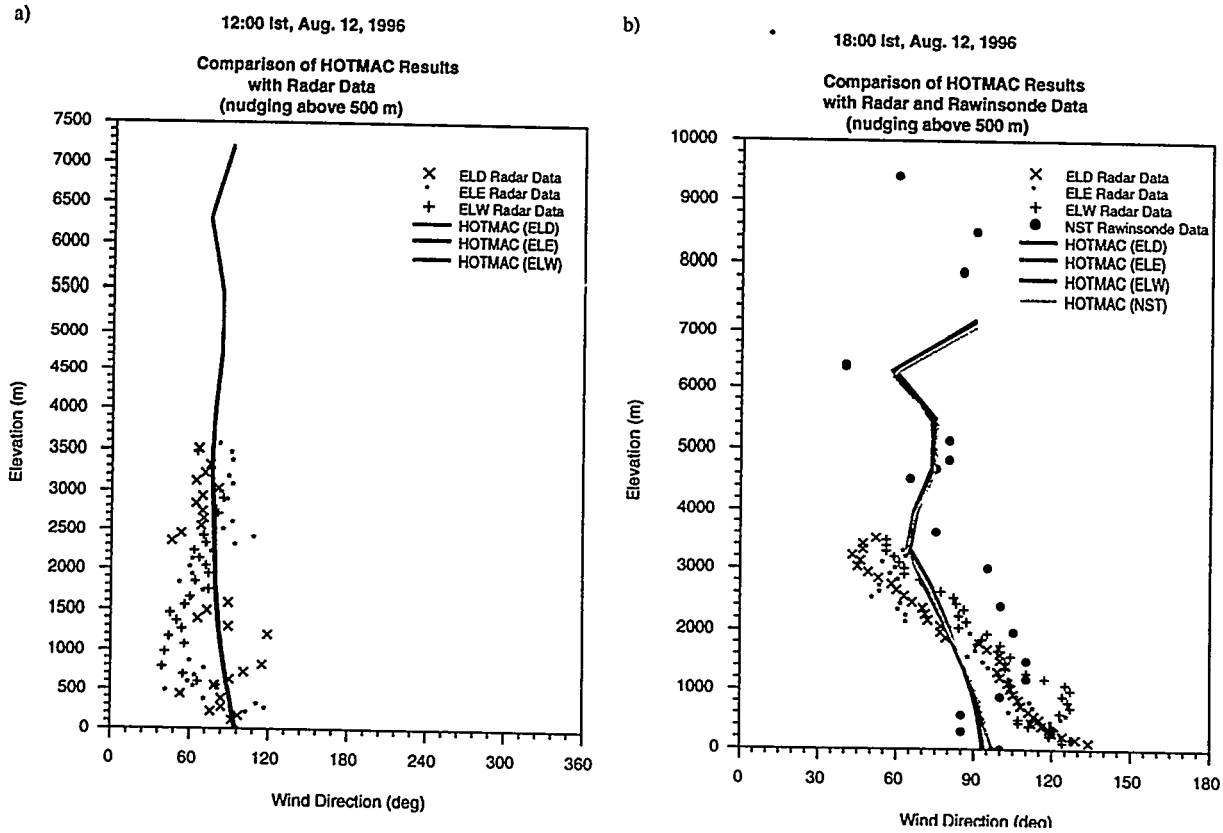

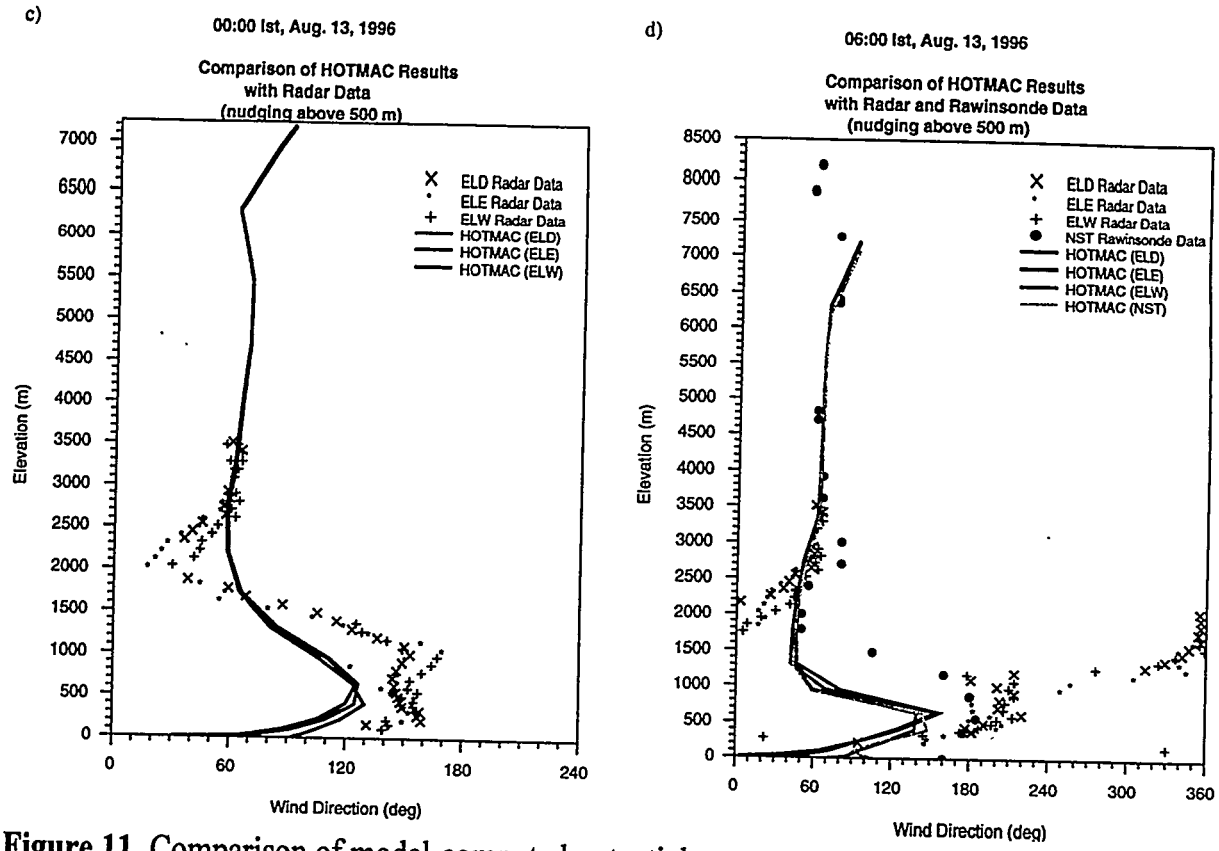

Figure 11. Comparison of model-computed potential temperature profiles and field measurements for: a) 12 noon, b) 6 pm, c) 12 midnight and d) 6 am.